# The crystal structure of the complex of $P_{II}$ and acetylglutamate kinase reveals how $P_{II}$ controls the storage of nitrogen as arginine

José L. Llácer*, Asunción Contreras†, Karl Forchhammer‡, Clara Marco-Marín*, Fernando Gil-Ortiz*§, Rafael Maldonado†, Ignacio Fita¶, and Vicente Rubio*‖

*Instituto de Biomedicina de Valencia–Consejo Superior de Investigaciones Cientificas (CSIC) and Centro de Investigación Biomédica en Red de Enfermedades Raras (CIBERER), Jaime Roig 11, 46010 Valencia, Spain; †División de Genética, Universidad de Alicante, Apartado de Correos 99, 03080 Alicante, Spain; ‡Lehrstuhl für Mikrobiologie/Organismische Interaktionen, University of Tübingen, Auf der Morgenstelle 28, D-72076 Tübingen, Germany; and ¶Instituto de Biología Molecular de Barcelona–CSIC and Institute for Research in Biomedicine, Josep Samitier 1-5, Parc Cientific, 08028 Barcelona, Spain

Edited by John Kuriyan, University of California, Berkeley, CA, and approved October 3, 2007 (received for review June 26, 2007)

**Photosynthetic organisms can store nitrogen by synthesizing arginine, and, therefore, feedback inhibition of arginine synthesis must be relieved in these organisms when nitrogen is abundant. This relief is accomplished by the binding of the $P_{II}$ signal transduction protein to acetylglutamate kinase (NAGK), the controlling enzyme of arginine synthesis. Here, we describe the crystal structure of the complex between NAGK and $P_{II}$ of *Synechococcus elongatus*, at 2.75-Å resolution. We prove the physiological relevance of the observed interactions by site-directed mutagenesis and functional studies. The complex consists of two polar $P_{II}$ trimers sandwiching one ring-like hexameric NAGK (a trimer of dimers) with the threefold axes of these molecules aligned. The binding of $P_{II}$ favors a narrow ring conformation of the NAGK hexamer that is associated with arginine sites having low affinity for this inhibitor. Each $P_{II}$ subunit contacts one NAGK subunit only. The contacts map in the inner circumference of the NAGK ring and involve two surfaces of the $P_{II}$ subunit. One surface is on the $P_{II}$ body and interacts with the C-domain of the NAGK subunit, helping widen the arginine site found on the other side of this domain. The other surface is at the distal region of a protruding large loop (T-loop) that presents a novel compact shape. This loop is inserted in the interdomain crevice of the NAGK subunit, contacting mainly the N-domain, and playing key roles in anchoring $P_{II}$ on NAGK, in activating NAGK, and in complex formation regulation by MgATP, ADP, 2-oxoglutarate, and by phosphorylation of serine-49.**

arginine synthesis | regulation | x-ray structure | signaling | cyanobacteria

In photosynthetic organisms nitrogen can be stored by synthesizing arginine (1, 2) and, therefore, feedback inhibition of arginine synthesis must be relieved when nitrogen is abundant. The enzyme of arginine biosynthesis that is the target of arginine inhibition, *N*-acetyl-L-glutamate (NAG) kinase (NAGK) (1, 3–5), was found in cyanobacteria and plants (2, 4–8) to be a target of the carbon/nitrogen $P_{II}$ signaling protein (9, 10), forming with it a complex in which arginine inhibition is alleviated (6, 7).

$P_{II}$ signaling proteins are homotrimers of a 12- to 13-kDa subunit that interact with enzymes, transcription factors, and ammonia channels, regulating their activity (9, 10) and carbon/nitrogen homeostasis. Numerous structures of $P_{II}$ proteins, including those for cyanobacteria and plants (9–12), are known, but it was unclear how $P_{II}$ proteins carry out their functions. The body of the $P_{II}$ trimer is roughly hemispheric. Its subunits have $\beta\alpha\beta\beta\alpha\beta$ topology, with $\alpha$ helices looking outward and the $\beta$ sheet inward and providing the intersubunit interactions. Each subunit has three loops: the B- and C-loops and the larger flexible T-loop. The T-loop residues Y51 and S49 are, respectively, the sites of the regulatory uridylylation and phosphorylation in enterobacterial and cyanobacterial $P_{II}$ proteins (9, 10), with S49 phosphorylation abolishing interaction with NAGK (4, 6). ADP, MgATP, and 2-oxoglutarate (2OG) bind at the T-loop (13) and modulate the binding of $P_{II}$ to its targets (6, 9, 10). The recently determined structure of the inhibitory complex of GlnK (a $P_{II}$ protein) with the ammonia channel AmtB of *Escherichia coli* (14, 15) showed that the extended T-loop blocks the cytoplasmic opening of the ammonia channel, explaining channel function inhibition. This structure sheds no light on the $P_{II}$–NAGK complex because $P_{II}$ activates NAGK (6, 7) and because ADP was found in the GlnK–AmtB complex (15), whereas ADP prevents $P_{II}$–NAGK complex formation (6).

We determine here the crystal structure of the $P_{II}$–NAGK complex of the cyanobacterium *Synechococcus elongatus* strain PCC7942. We previously determined the structures of arginine-insensitive (16) and arginine-sensitive NAGKs (17). The latter are hexameric ring-like trimers of dimers with a central hole of 25–30 Å, in which the dimers resemble the homodimeric arginine-insensitive enzyme (16). The NAGK subunit is an open $\alpha_3\beta_8\alpha_4$ sandwich that can be divided into a N-domain and a C-domain. The N- and C-domains host, respectively, the NAG and ATP sites, on the C-edge of the central $\beta$-sheet. Arginine-sensitive NAGKs (17) have a N-terminal mobile kinked $\alpha$-helix (called the N-helix) that, by interlacing with another dimer N-helix, links the dimers into the hexamer. The dimers are tilted relative to the ring plane, and the upper and lower ring surfaces are serrated, with three peaks, one per subunit. Arginine binds on each subunit next to the interdimeric junctions near the N-helices, widening the ring, decreasing the tilt of the dimers and reorienting the N-helices (17). In the present complex, the NAGK closely resembles other arginine-sensitive NAGKs. In contrast, the T-loop of $P_{II}$ adopts a novel compact shape that is specifically adapted to this interaction. We use site-directed mutagenesis, functional assays, and binding studies to confirm the *in vivo* relevance of this complex. The structure clarifies regulation of $P_{II}$ binding to NAGK and $P_{II}$ activation of NAGK. Sequence signatures identified here for $P_{II}$ signaling through

Author contributions: J.L.L. and V.R. designed research; J.L.L., A.C., K.F., R.M., and V.R. performed research; J.L.L., A.C., K.F., C.M.-M., F.G.-O., I.F., and V.R. analyzed data; and J.L.L. and V.R. wrote the paper.

The authors declare no conflict of interest.

This article is a PNAS Direct Submission.

Abbreviations: NAGK, *N*-acetyl-L-glutamate kinase; NAG, *N*-acetyl-L-glutamate; 2OG, 2-oxoglutarate.

The atomic coordinates and structure factors have been deposited in the Protein Data Bank, www.pdb.org [PDB ID codes 2V5H (crystal I) and 2JJ4 (crystal II)].

§Present address: Centro de Investigación Príncipe Felipe (CIPF), Avenida Autopista del Saler, E-46013 Valencia, Spain.

‖To whom correspondence should be addressed at: Instituto de Biomedicina de Valencia, Jaime Roig 11, Valencia 46010, Spain. E-mail: rubio@ibv.csic.es.

This article contains supporting information online at www.pnas.org/cgi/content/full/0705987104/DC1.

**Table 1. Data collection and refinement statistics**

| Parameter | Crystal I | Crystal II |
|---|---|---|
| Space group | $P2_1$ | $C222_1$ |
| Unit cell (*a*, *b*, *c*), Å | 90.4, 161.0, 91.6 | 106.9, 149.5, 162.2 |
| | $\beta$ = 106.5° | |
| Resolution, Å* | 87.71–2.75 | 54.07–3.46 |
| | (2.90–2.75) | (3.65–3.46) |
| Completeness, %* | 100 (100) | 100 (100) |
| Multiplicity* | 5.1 (5.2) | 4.1 (4.1) |
| $I/\sigma$* | 6.9 (2.0) | 6.3 (1.9) |
| $R_{sym}$, %* | 8.5 (36.7) | 9.9 (39.1) |
| Reflections, total/unique | 334,220/65,178 | 70,396/17,338 |
| $R_{cryst}/R_{free}$, % | 20.0/23.6 | 23.3/29.4 |
| rmsd bond length, Å | 0.011 | 0.010 |
| rmsd bond angles, ° | 1.37 | 1.13 |
| No. of atoms/average *B*-factors, Å$^2$ | | |
| Protein atoms | 17,902/38.3 | 8,531/73.4 |
| NAG | 6/45.7 | 2/73.2 |
| Water | 187/31.8 | |
| Ramachandran plot, % | | |
| Favored | 92.0 | 89.2 |
| Allowed | 7.8 | 10.2 |
| Generous | 0.2 | 0.4 |
| Disallowed | 0 | 0.2 |

*Values in parentheses are data for the highest-resolution shell.

NAGK account for the restriction of this signaling to photosynthetic organisms.

## Results

**Crystallization and Overall Structure of the Complex.** Crystal forms (Table 1) I and II, diffracted to 2.75- and 3.46-Å resolution, respectively. Phases were obtained for crystal II with molecular replacement using models of *Thermotoga maritima* NAGK (17) and of uncomplexed *S. elongatus* $P_{II}$ (11), yielding a solution consisting of three subunits of each protein in the asymmetric unit. In turn, the partially refined structure of crystal II was used for molecular replacement in crystal I, yielding one NAGK hexamer and two $P_{II}$ trimers in the asymmetric unit, forming the complex. All six subunits of each protein in the asymmetric unit have virtually identical structure.

The complex (Fig. 1) has 32 point group symmetry. Two $P_{II}$ trimers sandwich one NAGK trimer of dimers, with their threefold axes aligned. The same complex was generated in crystal II after application of a crystal symmetry, but we will refer to the higher resolution (2.75 Å) crystal I structure. The complex approximates a sphere of radius ≈53 Å. The $P_{II}$ trimers are at the poles and contact the NAGK hexamer inner circumference. $P_{II}$ is not packed tightly on NAGK. Each $P_{II}$ subunit interacts with one NAGK subunit, contacting the $\alpha_4$ region of NAGK toward its connection with the central sheet N-edge (Fig. 2). Two surfaces of each $P_{II}$ subunit mediate the contacts: the B-loop and the $\beta1$–$\alpha1$ connection are exposed in the $P_{II}$ trimer flat side and contact the NAGK subunit C-domain; and the T-loop is inserted in the interdomain crevice, making extensive contacts with the NAGK N-domain.

**NAGK and Its Arginine Site.** The ring-like hexameric NAGK contains one normally bound NAG molecule in each subunit (Fig. 2) and closely resembles other arginine-inhibitable NAGKs (17) [Figs. 1 and 2, and supporting information (SI) Fig. 5]. Superimposition of the dimers with those of *T. maritima* NAGK reveals (Fig. 3*A*) a rigid

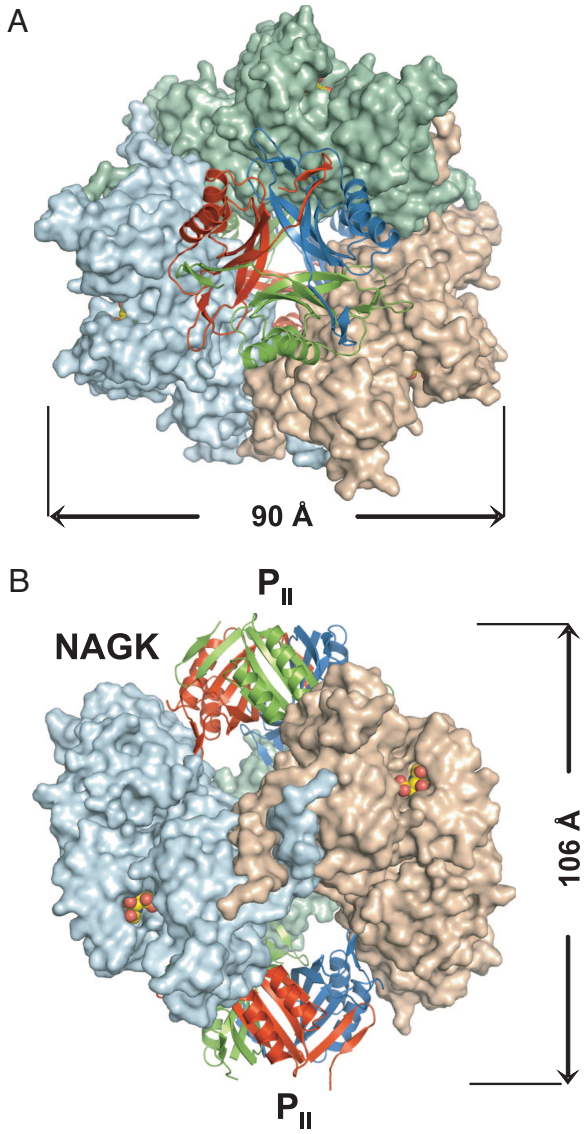


**Fig. 1.** $P_{II}$–NAGK complex. NAGK, $P_{II}$, and NAG are shown as surface, ribbons, and spheres, respectively. NAGK dimers and $P_{II}$ subunits are colored independently. Views are along the threefold axis (*A*) or the twofold axis (*B*).

body displacement of 1.9 Å of the C-domains toward the contacting $P_{II}$ molecules. The hexamer is less wide, and its dimers are more tilted than in the arginine-bound NAGK of *T. maritima* (SI Fig. 5). The orientation of the N-helices, identical in all of the subunits, represents an approximate average of the closely related orientations of these helices in the arginine-free NAGK of *Pseudomonas aeruginosa* (17) (Fig. 3*B*).

Each NAGK subunit exhibits one arginine site at its expected location (Fig. 3 *C* and *D*). This site is widened relative to the high affinity site of *T. maritima* NAGK (Fig. 3 *C* and *D*) because of movements of the elements forming the site. The N-helix C-terminal portion is positioned as in the empty site of *P. aeruginosa* NAGK, with the phenolic ring of Y23, which should accommodate the $C^{\alpha}$ of arginine (17), dislodged from the site. Strand $\beta16$ is moved toward the $P_{II}$ molecule that binds to its C-end, and the side chain of M287, which would stack the chain of bound arginine, is displaced away ≈1 Å. The $\alpha$H–$\beta16$ connecting loop, which would bind through its main-chain O atoms the guanidinium and $\alpha$-$NH_3^+$ groups of arginine, is overexpanded, possibly because of pulling by the N-helix of the

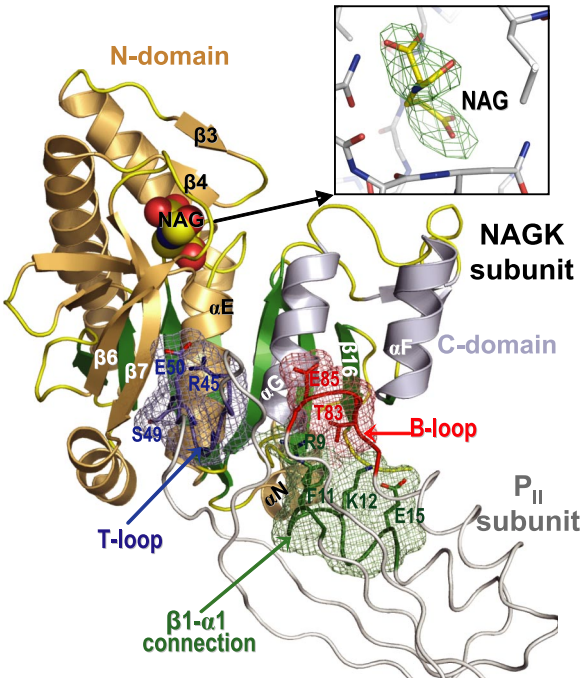


**Fig. 2.** $P_{II}$ subunit–NAGK subunit contacts. $P_{II}$, NAGK, and NAG are shown as strings, ribbons, and spheres, respectively. The contacting parts of the T-loop, B-loop, and $\beta1$–$\alpha1$ connection, including some interacting side chains (in sticks), are blue, red, and green, respectively. The surfaces provided by these elements form meshworks of the same colors. The NAGK central $\beta$-sheet is green, and other $\beta$-strands and the $\alpha$-helices are brownish and grayish for N- and C-domains, respectively. Some NAGK elements and $P_{II}$ residues are labeled. (*Inset*) Structure of bound NAG, encased within its electron density omit map contoured at 2.5$\sigma$.

other subunit that runs parallel to it (Fig. 3*D*). These arginine site changes justify the ≈15-fold increase in the half-inhibitory concentration of arginine ($I_{0.5}^{Arg}$) triggered by $P_{II}$ (Table 2 and SI Fig. 6).

**$P_{II}$ Exhibits a Compact T-Loop.** *S. elongatus* $P_{II}$ resembles closely the structure of free $P_{II}$ (11) (Fig. 4 *A–D*), except for the T-loop (residues 37–54), which, instead of being extended, is in all of the subunits in an identical compact conformation resembling a flexed leg having the proximal segment packed against the $P_{II}$ body and the distal segment (residues 41–52) packed against the proximal segment through a cushion of hydrophobic side chains (Y46, L56, and Y51) (Fig. 4*E*). Both segments are also linked by a salt bridge (E44–K58). In the distal segment, residues 44–51 form an imperfect $\beta$-hairpin that is centrally involved in the interactions with NAGK and that includes and exposes S49, the residue that when phosphorylated prevents complex formation (4, 6). A similarly shaped T-loop was observed very recently in GlnK1 of *Methanococcus jannaschii* bound to MgATP (13). Because the present complex has no nucleotides, each T-loop must be stabilized in the compact conformation by its contacts with NAGK. This compact conformation requires that a salt bridge between R47 and E85 (a B-loop residue) found in free $P_{II}$ (11) be broken, and, indeed, in the complex the partner of E85 in this bond is R233 of NAGK (Fig. 4*E*). Hydrogen bonds that link the main chain N atoms of R47 and G48 to the $\varepsilon$O atom of Q258 from NAGK (Fig. 4*E*) should stabilize this T-loop compact conformation. Contacts between the T- and B-loops (Q42 and E44 with I86) or even with helix 1 of the adjacent $P_{II}$ subunit also stabilize this compact conformation.

**Interaction of $P_{II}$ with NAGK.** The contacts with the C-domain of NAGK mediated by the flat side of the $P_{II}$ trimer, bury ≈304 Å$^2$ per $P_{II}$ subunit (determined with a probe of radius 1.4 Å) and involve the B-loop and the $\beta1$–$\alpha1$ junction (and adjacent residues) of $P_{II}$ and the N-end of helix F and the C-ends of helix G and of $\beta16$ (Fig. 2) of NAGK. These contacts include hydrophobic interactions (F11 and T83 of $P_{II}$ and I229, I253, and A257 of NAGK), hydrogen bonds, and the already mentioned bond between E85 of $P_{II}$ and R233 of NAGK. These interactions pull the C-domain and $\beta16$ toward $P_{II}$, contributing to the widening of the arginine site (see above) on the other side of the domain.

The other contact surface, provided by the T-loop terminal $\beta$-hairpin, buries 393 Å$^2$ per $P_{II}$ subunit. This hairpin is inserted at the NAGK interdomain crevice, being surrounded by and making contacts with the last turns of helix G, from the C-domain, and of helix E from the N-domain, as well as with the $\beta7$ strand of the $\beta6$–$\beta7$ hairpin at the N-domain surface (Figs. 2 and 4*F*). This last hairpin and the T-loop terminal hairpin form a hybrid imperfect four-stranded $\beta$-sheet involving five hydrogen bonds, of which two are provided by the OH group of S49. An ion-pair network (Fig. 4*F*) centered in the T-loop residues R45 and E50 (themselves connected by a salt bridge) radiates to the surrounding elements of NAGK, involving R139, D142, E151, E194, and R254, and possibly mediating the decrease in the $K_m^{NAG}$ induced by $P_{II}$ in the absence of arginine (see *Discussion*).

Overall, the $P_{II}$–NAGK interface is remarkably open, being composed of six small contact surfaces for each $P_{II}$ trimer, totaling 2,094 Å$^2$ buried area, or, for the NAGK hexamer, 1,826 Å$^2$ buried area per $P_{II}$ trimer. These buried surfaces only represent 14.3% of the exposed surface of $P_{II}$ and, for both $P_{II}$ trimers, only 5.8% of the exposed surface of the NAGK hexamer, accounting for the transient nature of the interactions between NAGK and $P_{II}$.

**Signature Sequences for $P_{II}$–NAGK Signaling.** The restriction to photosynthetic organisms of $P_{II}$–NAGK signaling reflects sequence and structural specializations. The T-loop residues R45 and S49 and the B-loop residue E85 have paramount roles in complex formation (Fig. 4 *E* and *F*) and are conserved in photosynthetic organisms but not in other organisms. The same applies to the NAGK residues E194, R233, R254, and Q258 of NAGK, all involved in the interactions (Figs. 4 *E* and *F*), and to A257, which centers the hydrophobic patch linking both proteins. The simultaneous presence of these residues in either $P_{II}$ or NAGK is a signature for the involvement of these proteins in $P_{II}$–NAGK signaling: these residues did not concur in any of 214 or 183 available $P_{II}$ or NAGK sequences from nonphotosynthetic organisms, but they were present in 46 of 48 and in 41 of 43 available $P_{II}$ and NAGK sequences of photosynthetic organisms (Swiss-Prot database; www.expasy.org). The two red algae without the NAGK signature, *Gracilaria tenuistipitata* and *Cyanidioschyzon merolae* (Swiss-Prot files Q6B8Z0 and Q85FW5, respectively) have no $P_{II}$ gene in their chloroplast genomes (National Center for Biotechnology Information genomes database files NC_006137 and NC_004779; www.ncbi.nlm.nih.gov/sites/entrez) and may not use $P_{II}$ signaling.

**Functional Relevance of the Complex Revealed by Site-Directed Mutagenesis and Binding Studies.** Using the yeast two-hybrid system that revealed the $P_{II}$–NAGK interaction (5), we detected no interaction between wild-type NAGK and the $P_{II}$ mutants F11A, R45A, Y46A, R47A, S49A, S49D, S49E, and E85A, or between wild-type $P_{II}$ and the NAGK mutants R139A, I229A, R233A, R254A, L256A, and Q258A (SI Fig. 7), whereas interaction between $P_{II}$ subunits or between NAGK subunits were not hampered by these mutations. All of these residues (except Y46 and L256, which are indirectly involved) are directly involved in $P_{II}$–NAGK contacts. In contrast, mutations to alanine of 7 $P_{II}$

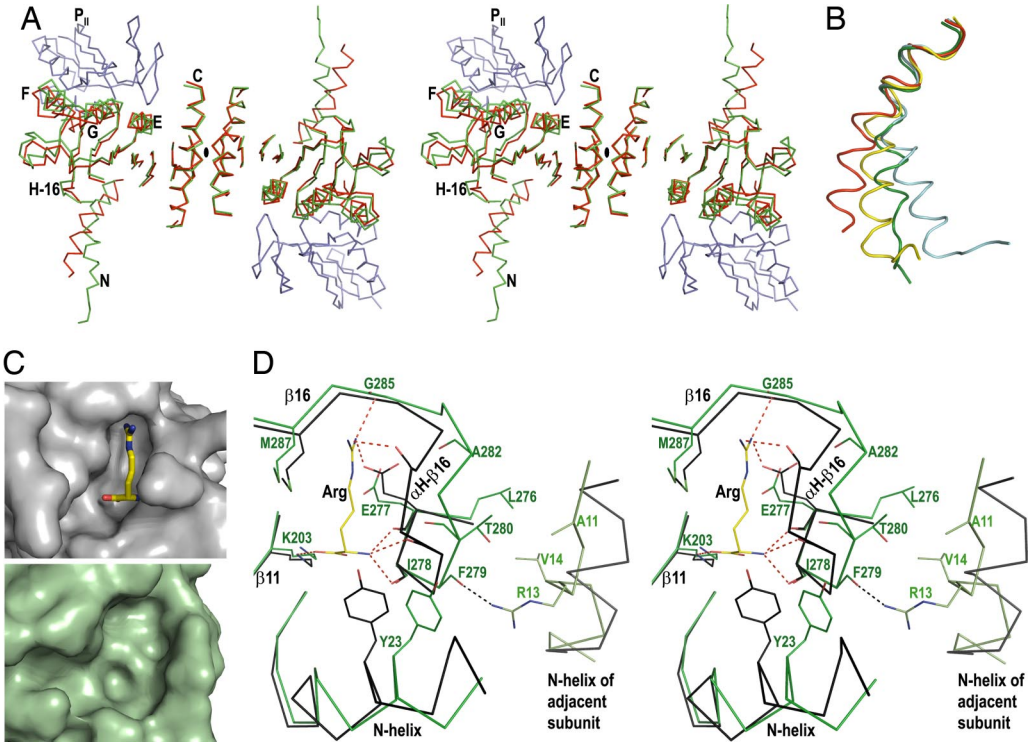


**Fig. 3.** Changes in the NAGK dimer, the N-helix, and the arginine site. (*A*) Stereoview of backbone superimposition of NAGK dimers of *S. elongatus* (green) and *T. maritima* (red). Two $P_{II}$ subunits (blue; labeled $P_{II}$) are bound to *S. elongatus* NAGK. The twofold axis (black ellipse) is perpendicular to the paper. For clarity, not all elements are shown in NAGK. Note the displacement toward $P_{II}$ of the C-domain and the opposite displacement of the N-helix, of *S. elongatus* NAGK. (*B*) N-helix orientation in the NAGKs of *S. elongatus* (green), *T. maritima* (red), and in two NAGK subunits of *P. aeruginosa* (cyan and yellow). (*C*) Arginine site surface in *T. maritima* NAGK (*Upper*) with bound arginine (in sticks) and in *S. elongatus* NAGK (*Lower*). (*D*) Stereoview of the superimposed arginine sites of *T. maritima* (black; bound arginine in yellow) and *S. elongatus* (green) NAGKs. The next subunit N-helix portion (in fainter color) runs parallel to the αH–β16 loop. Red broken lines are polar contacts with arginine, and the black broken line is one hydrogen bond between the αH–β16 loop and the adjacent subunit N-helix.

residues and 15 NAGK residues mapping at points of the molecular surfaces not directly involved in $P_{II}$–NAGK interactions did not prevent complex formation (SI Fig. 7, in blue). Thus, residues involved in the contacts in the crystalline complex are important residues for complex formation *in vivo*.

NAGK activity assays (Table 2) revealed that the $P_{II}$ mutations F11A, F11Q, R45A, S49D, or E85A, or the NAGK mutations R139A, I229A, I229N, R233A, or R254A abolished or greatly reduced the increase in the $I_{0.5}^{Arg}$ triggered by $P_{II}$ when using the wild-type proteins (Table 2). For most of these mutants, including the inactive (although soluble and hexameric) Q258A NAGK mutant, surface plasmon resonance assays showed abolished or decreased $P_{II}$–NAGK binding (Table 2). Because these mutations affect residues in which the side chains are directly involved in the $P_{II}$–NAGK contacts, the complex reflects the genuine interactions between NAGK and $P_{II}$. R47 of $P_{II}$ only contacts NAGK through its main-chain atoms, and Y46 of $P_{II}$ and L256 of NAGK are not directly involved in the contacts, and thus, the mutations at these residues had less important (R47 and Y46) or no (L256A) effect. As expected, the NAGK mutant D250A, used as an internal negative control, behaved just as did wild-type NAGK. Overall, the three assays agree and leave little doubt that the present complex reflects the physiological interactions between $P_{II}$ and NAGK. Further, the 2:1 $P_{II}$ trimer:NAGK hexamer stoichiometry of the complex is the same in the crystal and in solution, as shown in binding studies in which we used ultrafiltration to separate free $P_{II}$ from NAGK-complexed $P_{II}$, carried out with accurately quantitated protein solutions (see *SI Experimental Procedures*). The linear Scatchard plots (SI Fig. 8) revealed a single type of site occurring in a number of ≈2 per NAGK hexamer.

## Discussion

This work reveals how $P_{II}$ and NAGK interact while also describing the structure of *S. elongatus* NAGK and a novel conformation of the $P_{II}$ protein from this organism. The NAGK closely resembles other arginine-sensitive NAGKs (17) and appears representative of plant NAGKs, which are hexameric and similar in subunit mass (7, 18) and sequence (≈60% identity). Because plants and cyanobacteria have highly similar $P_{II}$ proteins (11, 12) and conserve key interacting residues, the present structure should also represent the complex in plants.

The importance of the compact T-loop conformation for complex formation is highlighted by the involvement of three of the eight residues of the $P_{II}$–NAGK signaling signature (E85 of $P_{II}$ and R233 and Q258 of NAGK) in triggering or in stabilizing the compact T-loop shape. By similarity with *M. jannaschii* GlnK1, MgATP, and ADP binding to $P_{II}$ should trigger, respectively, the compact and highly extended T-loop conformations (13, 15), explaining the dissociation of the $P_{II}$–NAGK complex by ADP but not by MgATP (6). These MgATP and ADP effects on the T-loop fit the proposed $P_{II}$ role in energy signaling in cyanobacteria (10).

Nitrogen abundance is signaled by $P_{II}$ through the inversely related 2OG levels (10), but there is conflict on the 2OG effects on NAGK-mediated signaling: 2OG hampered $P_{II}$–NAGK complex formation in plasmon resonance assays (6) but not in pulldown or gel filtration assays (4), and it slightly increased instead of decreasing NAGK activity in the presence of $P_{II}$ (4). With *Arabidopsis thaliana* proteins (7), 2OG did not prevent $P_{II}$-triggered increase in $I_{0.5}^{Arg}$. Because the structure of *M. jannaschii* GlnK1 (13) suggested that 2OG binding may stabilize the compact T-loop conformation triggered by MgATP (13),

**Table 2. Influence of mutations of $P_{II}$ or of NAGK on the arginine concentration causing 50% inhibition of NAGK ($I_{0.5}^{Arg}$) in the presence of $P_{II}$ and on surface plasmon resonance assay of $P_{II}$–NAGK complex formation**

| $P_{II}$ form | NAGK form | $I_{0.5}^{Arg}$, $\mu$ M* | Plasmon resonance signal, % |
|---|---|---|---|
| None | Wild type | 39 | 0 |
| Wild type | Wild type | 572 | 100 |
| F11A | Wild type | 46 | 0 |
| F11Q | Wild type | 52 | Not assayed |
| R45A | Wild type | 41 | 0 |
| Y46A | Wild type | 376 | 43 |
| R47A | Wild type | 380 | 16 |
| S49D | Wild type | 52 | 0 |
| E85A | Wild type | 91 | 4 |
| Wild type | R139A | 33 ± 12 | 10 |
| Wild type | I229A | 10 ± 9 | Not assayed |
| Wild type | I229N | 100 | Not assayed |
| Wild type | R233A | 65 ± 4 | 0 |
| Wild type | D250A | 466 | 100 |
| Wild type | R254A | 128 | 12 |
| Wild type | L256A | 517 | 100 |
| Wild type | Q258A | No activity | 0 |

The $I_{0.5}^{Arg}$ value was determined from plots of NAGK activity vs. arginine concentration, in assays containing 6 $\mu$g/ml NAGK (29 nM hexamer) and 2.4 $\mu$g/ml $P_{II}$ (65 nM trimer). The NAGK mutations did not alter substantially the $I_{0.5}^{Arg}$ in the absence of $P_{II}$, except for mutation L256A ($I_{0.5}^{Arg}$ in the absence of $P_{II}$, 115 ± 13 $\mu$M). For Biacore surface plasmon resonance, $His_6$-tagged NAGK proteins were immobilized on $Ni^{2+}$-nitrilotriacetic acid sensor chips, and $P_{II}$ proteins (87.5 $\mu$g/ml, 2.37 $\mu$M trimer) were the analytes.

*Unless indicated, standard errors did not exceed 5% of the mean values given.

2OG may not abolish $P_{II}$–NAGK interaction. However, the increased negative potential caused by 2OG binding (13) may hamper complex formation by electrostatic repulsion, given the negative potential of the NAGK ring faces (data not shown). This electrostatic effect should be strongly influenced by the ionic strength, possibly accounting for the variable 2OG effects in different assays (4, 6).

In *S. elongatus*, the phosphorylation of S49 of $P_{II}$ is stimulated by 2OG and prevents $P_{II}$ binding to NAGK (10). The present structure clarifies this effect of S49 phosphorylation. One donor hydrogen bond formed with NAGK by the S49 OH group is lost upon phosphorylation. More importantly, steric and electrostatic clash with NAGK binding should be triggered by the bulkiness and negative charge of the phosphate, given the involvement of S49 in the contacts with NAGK and the negative potential of the NAGK surface (data not shown).

Protein–protein complex formation involves an initial encounter complex in which one or few side chains of one protein act as anchors (19). The only residue in the complex that meets all of the characteristics of an anchor is the T-loop residue R45 (19): it belongs to the smaller protein, and it is exposed in the unbound form; it binds a preformed groove in the receptor, burying a positively charged (and thus polar) group and >100 Å$^2$ (115 Å$^2$ in the case of R45) of solvent-accessible surface. R45 is a key element of the ion-pair network linking the T-loop and NAGK. This network may mediate the decrease in the $K_m^{NAG}$ triggered by $P_{II}$ on *S. elongatus* NAGK in the absence of arginine. The network involves D142, which stems from a loop that is glued to the mobile lid of the NAG site (Fig. 4*F*). The pull on D142 toward $P_{II}$ upon network completion may drag the lid toward its lowered position (16, 17) found in the high-affinity form of the NAG site. This action explains why the lid is lowered in an empty NAG site of crystal II (data not shown), and the lack of effect

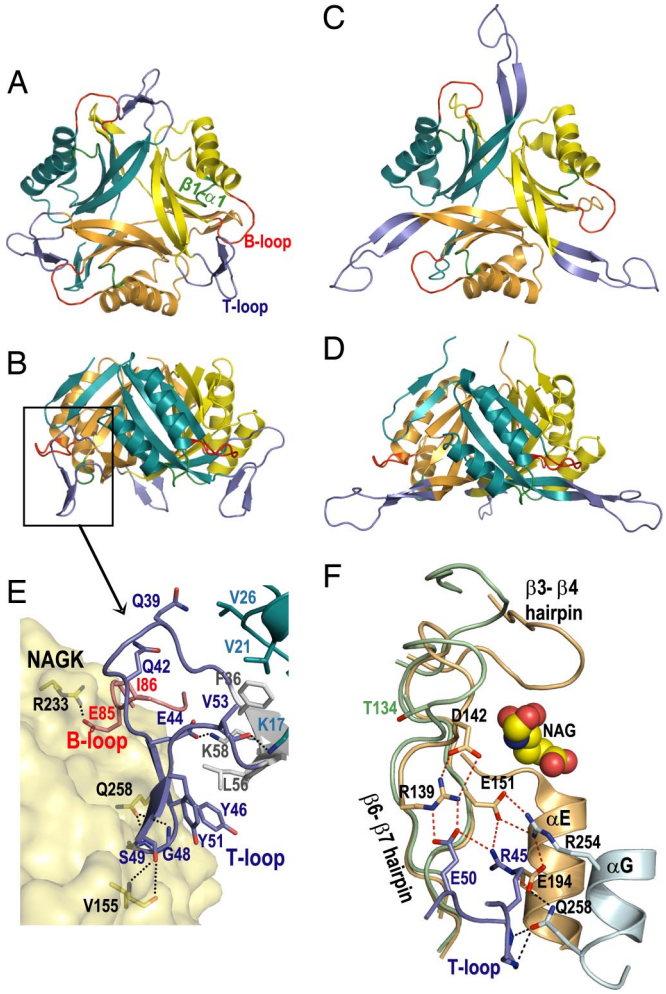


**Fig. 4.** The $P_{II}$ trimer and the T-loop. (*A–D*) Ribbon representations of the trimer, with independent coloring of each subunit, except the T-loop, B-loop, and $\beta$1–$\alpha$1 junction, colored blue, red, and green, respectively. The $P_{II}$ conformation in the present complex (*A* and *B*) and in free *S. elongatus* $P_{II}$ (*C* and *D*), are compared. Views are along the threefold axis from the side that contacts NAGK (*A* and *C*) or perpendicularly to the vertical threefold axis, with the face that interacts with NAGK looking down (*B* and *D*). (*E*) T-loop (in blue) contacts with NAGK subunit (yellow semitransparent surface) showing interacting residues. Parts of the B-loop (in red) and of another $P_{II}$ subunit (green) that interact with the T-loop are also represented. (*F*) Ion-pair network (red broken lines) centered in the T-loop (blue), involving NAGK subunit N-domain (yellow) and C-domain (grayish) elements. The $\beta$6–$\beta$7 hairpin and the neighboring $\beta$3–$\beta$4 hairpin forming the NAG site lid (with bound NAG as spheres) are in string representation and are compared with the corresponding hairpins of *T. maritima* NAGK (in green). Residue side chains are shown as sticks and hydrogen bonds as black broken lines.

of $P_{II}$ on the $K_m^{NAG}$ in the absence of arginine in the NAGK of *A. thaliana* (7), which has D142 replaced by Asn.

The present structure clarifies how $P_{II}$ binding renders NAGK less sensitive to arginine. Given the low activity and high apparent affinity for arginine of *S. elongatus* NAGK in the absence of $P_{II}$ and its increased activity and decreased affinity for arginine in the complex with $P_{II}$ (4, 6), the binding of $P_{II}$ must stabilize an active NAGK form having low affinity for arginine. Previous work (17) with other NAGKs equated this form with a narrow-ring conformation of the NAGK hexamer presenting highly tilted dimers and an orientation of the interlaced N-helices that is restricted within narrow spatial margins. The NAGK in the present complex conforms with these requirements for narrowness, high dimer tilt (SI Fig. 5), and N-helices

orientation (Fig. 3*B*). Through their linkage to $P_{II}$, the NAGK subunits should be pulled toward both poles of the complex, favoring the high tilt of the NAGK dimers and the concomitant narrowing of the NAGK ring, and indirectly forcing the N-helices that interconnect the dimers into the observed orientation, associated with a low-affinity form of the arginine site. In addition, the interactions of the $P_{II}$ body with the C-domains of NAGK pull from $\beta$16, contributing to arginine site widening. In any case, the effects of $P_{II}$ on NAGK functionality are long-distance effects because they do not involve $P_{II}$ participation in substrate sites or $P_{II}$ occlusion of the arginine site. This fact fits the observation that the increase in $I_{0.5}^{Arg}$ is saturated with increasing $P_{II}$ concentrations (SI Fig. 6): there should not be such saturation for physical competition between $P_{II}$ and arginine for the arginine site.

The binding of two $P_{II}$ trimers per NAGK hexamer revealed by the present structure and binding studies fits prior determinations with *S. elongatus* NAGK and $P_{II}$ (6), provided that these earlier data are corrected for apparent NAGK overestimation by a factor of 1.73 (caused by the use in ref. 6 of a too small $\varepsilon^{280}$ for NAGK). A stoichiometry of 1:1 $P_{II}$ trimer:NAGK hexamer reported (7) for the complex of *A. thaliana* may need revision because molar concentrations of the proteins may not have been accurate and because the assays involved potentially damaging long incubations at 25°C. Clearly, our crystallographic evidence and binding assays strongly indicate that each NAGK molecule has two apparently identical sites for $P_{II}$. Considering the abundance of $P_{II}$ in *S. elongatus* (K.F., unpublished data), NAGK should mainly exist in complex with two $P_{II}$ trimers when nitrogen is abundant.

The indirect effects of $P_{II}$ on NAGK functionality contrast with the direct role of GlnK in blocking the ammonia channel AmtB (14, 15). In the latter case, the tip of the ADP-binding and more extended T-loop, including nonuridylylated Y51, blocks the cytoplasmic opening of the channel. As in the complex with NAGK, the flat side of the GlnK trimer looks toward the target, but nearly all of the contacts are mediated by the T-loop, the anchor residue appears to be R47, and the T-loop conformation resembles one conformation of the ADP-bound loop of *M. jannaschii* GlnK1 (13). More examples of structures of $P_{II}$ complexed to other targets will have to be characterized to ascertain whether the present structure and that of the GlnK–AmtB complex are paradigms for the interaction of $P_{II}$ with its targets, or whether $P_{II}$ is a highly plastic protein that is able to adapt its T-loop in diverse ways for interaction with different targets.

## Experimental Procedures

Full protocols are available in *SI Experimental Procedures*.

**Preparation of $P_{II}$ and NAGK.** The *argB* and *glnB* genes of *S. elongatus* strain PCC7942, encoding NAGK and $P_{II}$, were PCR-cloned from plasmids pUAGC62 and pUAGC12 (5), respectively, in the NdeI and XhoI or NdeI and HindIII sites of pET-15b or pET-22b plasmids, being separately expressed in *E. coli* BL21 cells. Purification of N-terminally His-tagged NAGK (N-terminal sequence $MGSSH_6SSGLVPRGSHM$, ending in M1 of wild-type NAGK) and of $P_{II}$ were described previously (6, 11).

**Crystallization of the Complex.** A mixture of 0.5 mg/ml NAGK and 0.1 mg/ml $P_{II}$, in a solution containing 20 mM Hepes (pH 7.5), 1 mM DTT, 40 mM NaCl, 10 mM $MgCl_2$, and 20 mM NAG, incubated for 10 min at 23°C, was concentrated to 5 mg/ml by ultrafiltration. The complex was crystallized in two forms (Table 1) at 21°C in hanging drops made of 1 $\mu$l each of protein and precipitant solution [crystal I: 0.1 M Tris·HCl, pH 8.5/0.15 M sodium acetate/20% (wt/vol) polyethylene glycol 4000; crystal II: 0.1 M sodium cacodylate, pH 6.5/0.25 M magnesium acetate/10% (wt/vol) polyethylene glycol 8000].

**Data Collection and Structure Determination.** For details, see Table 1 and *SI Experimental Procedures*.

**Other Methods.** Site-directed mutagenesis of yeast two-hybrid plasmids (5) was carried out by using the QuikChange II system from Stratagene (La Jolla, CA) according to the manufacturer's instructions. Yeast two-hybrid analysis of NAGK and $P_{II}$ mutants was carried out as described previously (5). For activity and plasmon resonance assays (4, 6), the *argB* and *glnB* mutants were PCR-subcloned into, respectively, pET-22b and the *Strep* tag fusion vector pASK-IBA3 (IBA GmbH, Göttingen, Germany), and the mutant proteins were overexpressed and purified (4, 6). When comparing with these mutants, wild-type $P_{II}$ was also fused to the *Strep* tag II peptide (4). All of the purified mutants of $P_{II}$ and NAGK were soluble and formed the expected oligomer (checked by PAGE under nondenaturing conditions). The binding of $P_{II}$ to NAGK was quantitated by centrifugal ultrafiltration through a membrane cutoff of 100 kDa, monitoring the decrease in the amount of $P_{II}$ crossing the membrane when NAGK was added.

We thank I. Fuentes and M. Maheswaran for technical help. This work was supported by Spanish Ministry of Education and Science Grants BFU2004-05159, BFU2005-02231, and DFG Fo195/4. J.L.L. is a fellow of the Spanish Ministry of Education and Science. European Union and European Synchotron Radiation Facility (ESRF) Grenoble gave financial support for synchrotron use, and ESRF personnel provided expert help.

1. Slocum RD (2005) *Plant Physiol Biochem* 43:729–745.
2. Maheswaran M, Ziegler K, Lockau W, Hagemann M, Forchhammer K (2006) *J Bacteriol* 188:2730–2734.
3. Fernández-Murga ML, Gil-Ortiz F, Llácer JL, Rubio V (2004) *J Bacteriol* 186:6142–6149.
4. Heinrich A, Maheswaran M, Ruppert U, Forchhammer K (2004) *Mol Microbiol* 52:1303–1314.
5. Burillo S, Luque I, Fuentes I, Contreras A (2004) *J Bacteriol* 186:3346–3354.
6. Maheswaran M, Urbanke C, Forchhammer K (2004) *J Biol Chem* 279:55202–55210.
7. Chen YM, Ferrar TS, Lohmeier-Vogel EM, Morrice N, Mizuno Y, Berenger B, Ng KK, Muench DG, Moorhead GB (2006) *J Biol Chem* 281:5726–5733.
8. Sugiyama K, Hayakawa T, Kudo T, Ito T, Yamaya T (2004) *Plant Cell Physiol* 45:1768–1778.
9. Arcondeguy T, Jack R, Merrick M (2001) *Microbiol Mol Biol Rev* 65:80–105.
10. Forchhammer K (2004) *FEMS Microbiol Rev* 28:319–333.
11. Xu Y, Carr PD, Clancy P, Garcia-Dominguez M, Forchhammer K, Florencio F, Vasudevan SG, Tandeau De Marsac N, Ollis DL (2003) *Acta Crystallogr D* 59:2183–2190.
12. Mizuno Y, Berenger B, Moorhead GB, Ng KK (2007) *Biochemistry* 46:1477–1483.
13. Yildiz O, Kalthoff C, Raunser S, Kuhlbrandt W (2007) *EMBO J* 26:589–599.
14. Gruswitz F, O'Connell J, III, Stroud RM (2007) *Proc Natl Acad Sci USA* 104:42–47.
15. Conroy MJ, Durand A, Lupo D, Li XD, Bullough PA, Winkler FK, Merrick M (2007) *Proc Natl Acad Sci USA* 104:1213–1218.
16. Ramon-Maiques S, Marina A, Gil-Ortiz F, Fita I, Rubio V (2002) *Structure (London)* 10:329–342.
17. Ramon-Maiques S, Fernandez-Murga ML, Gil-Ortiz F, Vagin A, Fita I, Rubio V (2006) *J Mol Biol* 356:695–713.
18. Lohmeier-Vogel EM, Loukanina N, Ferrar TS, Moorhead GB, Thorpe TA (2005) *Plant Physiol Biochem* 43:854–861.
19. Rajamani D, Thiel S, Vajda S, Camacho CJ (2004) *Proc Natl Acad Sci USA* 101:11287–11292.